On the Determination of Internal-wave Directional Spectra from Moored Instruments[1]

Friedrich Schott and Jürgen Willebrand

Institut für Meereskunde
an der Universität Kiel
23 Kiel, Germany

ABSTRACT

Presented here is a model for determining the characteristic parameters of an internal-wave field using cross spectra of data obtained from vertically separated and/or horizontally separated moored instruments. The model is based on the assumption that the motion consists mainly of linear free internal waves having random phase relationships. The internal-wave energy is supposed to be distributed among a finite number of modes having continuous directional distribution. The free parameters of the theoretical cross-spectral function for such a wave field (i.e., the modal energies, mean propagational directions, and beam widths) are obtained by a least-squares fit to the observed cross spectra between all components of motion. Error calculations for the determined parameters are given. The number of degrees of freedom in this fitting procedure is high; e.g., 91 for a three-mode fit to current data from five stations.

The method is applied to records of tidal waves obtained in both shallow and deep water. The cross spectra and the spatial coherence field of current and temperature data obtained from an array in the North Sea could well be explained by a tidal-wave field that consists of the barotropic mode and the first baroclinic mode. For the current cross spectra derived from a mooring in the deep sea near the Great Meteor Seamount, additionally a second baroclinic mode was needed for the cross-spectral fit; in this case, however, the approximation was not as good as in the shallow-water example, probably due to the influence of the nearby seamount.

Within the limitations of the model, the cross-spectral fit can be easily applied to all kinds of internal-wave data, once the cross spectra and the eigenfunctions are determined.

1. *Introduction.* In the past decade, the theory of internal waves has been developed notably. However, there still is a large gap between the various theoretical models that deal with the generation and propagation of internal waves in the ocean and the practical possibilities to verify their results from observations. For a comparison of theory with oceanic observations the knowl-

1. Accepted for publication and submitted to press 15 February 1973.

edge of the actual directional-energy spectrum is a basic requirement. The determination of internal-wave directional spectra is complicated mainly by two facts: First, the horizontally separated instruments will never be sufficient in number to permit a straight-forward computation; the difficulties are increased by the modal structure of the internal waves. Second, the time scales of the generating processes of internal waves (e.g., wind-field changes) cannot be expected to be long against the investigated periods of the wave motion.

Different methods have been applied to obtain the internal wave-field parameters from time series of current and temperature fluctuations measured with moored oceanographic sensors. Some of these methods treat the three components of motion independently while some combine the horizontal components. Most of the methods are confined to special cases that employ only horizontally or vertically separated instruments.

There have been few experiments undertaken with horizontally separated instruments that recorded data simultaneously. Zalkan (1970) measured temperature fluctuations with a triangular array of 30-m sidelength from FLIP and tried to explain the horizontal phase differences with a single-plane wave. Schott (1971a, 1971b) ascertained the parameters of thermocline waves of tidal and inertial period by using the cross spectra of temperature fluctuations observed at four moorings in the North Sea. Wunsch and Hendry (1972) measured near-bottom currents with three horizontally separated moorings on the continental slope south of Cape Hatteras; they estimated the directional spectra of the tidal-current components by using the conventional method and a recently developed high-resolution method (Capon 1969). Thus, the various methods permit only the location of the main energy maximum in the wave-number plane because of the limited number of stations; they do not provide much information on modal structure and directional distribution.

Many records derived from vertically distributed instruments at single stations in both shallow and deep water have been obtained. From such data, the amplitudes and phases of internal-wave modes can be calculated by fitting eigenfunctions to the individual current components or to the vertical elevation, calculated from temperature or salinity fluctuations. For example, Krauss (1963) determined internal-seiche modes from current measurements in the Baltic; Magaard and McKee (in press) analyzed internal tides from current records obtained for two months at Site D in the North Atlantic.

Munk and Phillips (1968) were the first to combine the properties of horizontal-wave propagation and the vertical-mode structure. Garrett and Munk (1972) explained the gross features of all the observed moored frequency spectra and towed wave-number spectra by means of an isotropic multimode internal-wave model. However, the two models are not designed primarily for determining the details of the directional spectrum of single events.

Our aim here is to present a data-handling procedure that will determine the energy distribution on each mode from horizontally and vertically distrib-

uted instruments. The data that seem to be most suitable for this purpose are the cross spectra between all observed components of motion. We calculate theoretical cross spectra as functions of free parameters that are adjusted to fit the observed quantities in a least-squares sense and that determine the directional spectrum. Furthermore, these parameters may help to explain the spatial coherence field in the ocean. The underlying assumption is that the motion can be described mainly by a statistical field of free internal waves that is stationary in time and is horizontally homogeneous. Thus, the different internal-wave modes have no fixed phase relationships. This assumption is supported by many oceanic observations, all of which indicate a coherence loss over relatively small vertical separations (Perkins 1970, Siedler 1971, Webster 1972) and horizontal distances (Krauss 1969, Siedler [in press], Wunsch and Dahlen 1970, Wunsch and Hendry 1972).

2. *Cross Spectra and Directional Spectrum.* We start with the linearized hydrodynamic equations with arbitrary density stratification; we neglect compressibility, viscosity, and diffusion and use the Boussinesq approximation and the "traditional approximation" for the Coriolis force (Eckart 1960). Furthermore, we assume a constant depth and a vanishing mean current. The time series available for directional spectral analysis are the horizontal current fluctuations, u, v (east and north, respectively), and the vertical displacement, ζ.[2] These quantities may be represented by their Fourier sums:

$$\begin{matrix} u(\boldsymbol{x},z,t) = \\ v(\boldsymbol{x},z,t) = \\ \zeta(\boldsymbol{x},z,t) = \end{matrix} \begin{pmatrix} \xi_1 \\ \xi_2 \\ \xi_3 \end{pmatrix} = \sum_{\boldsymbol{k},\omega} \begin{pmatrix} \frac{1}{k}\tilde{u}(\boldsymbol{k},\omega)\frac{d}{dz}\psi(k,\omega,z) \\ \frac{1}{k}\tilde{v}(\boldsymbol{k},\omega)\frac{d}{dz}\psi(k,\omega,z) \\ \tilde{\zeta}(\boldsymbol{k},\omega)\psi(k,\omega,z) \end{pmatrix} e^{i(\boldsymbol{kx}-\omega t)}, \qquad (2.1)$$

with $\boldsymbol{x}$ the horizontal coordinate vector and z the vertical coordinate. The eigenfunctions $\psi(k,\omega,z)$ are determined from

$$\frac{d^2\psi}{dz^2} + k^2\frac{N^2(z)-\omega^2}{\omega^2-f^2}\psi = 0, \qquad (2.2)$$

with appropriate boundary conditions. For convenience we use the notation

$$\left.\begin{aligned} \varphi_1(k,\omega,z) = \varphi_2(k,\omega,z) &= \frac{1}{k}\frac{d}{dz}\psi(k,\omega,z) \\ \varphi_3(k,\omega,z) &= \psi(k,\omega,z). \end{aligned}\right\} \qquad (2.3)$$

2. In practice, ζ has to be calculated from temperature or salinity measurements.

The Fourier amplitudes of current components and vertical displacement are related by

$$\left.\begin{aligned}\tilde{u}(\boldsymbol{k},\omega) &= -(\omega\sin\Phi + if\cos\Phi)\,\tilde{\zeta}(\boldsymbol{k},\omega),\\ \tilde{v}(\boldsymbol{k},\omega) &= (if\sin\Phi - \omega\cos\Phi)\,\tilde{\zeta}(\boldsymbol{k},\omega),\end{aligned}\right\} \tag{2.4}$$

where Φ is the direction of the wave-number vector, $\boldsymbol{k}$, counted clockwise from the north, and f is the inertial frequency. The covariance matrix is given by

$$H^{mn}(\boldsymbol{r},z,z',\tau) = <\xi_m(\boldsymbol{x},z,t)\cdot\xi_n(\boldsymbol{x}+\boldsymbol{r},z',t+\tau)>, \tag{2.5}$$

where $<\ldots>$ denotes the ensemble average. With (2.1) to (2.3), H^{mn} may be written in terms of the Fourier components:

$$\left.\begin{aligned}H^{mn}(\boldsymbol{r},z,z',\tau) = \sum_{k,\omega} &<\tilde{\zeta}(\boldsymbol{k},\omega)\,\tilde{\zeta}^*(\boldsymbol{k},\omega)>\, T^{mn}(\Phi,\omega)\cdot\\ &\cdot R^{mn}(k,\omega,z,z')\,e^{-i(\boldsymbol{kr}-\omega\tau)},\end{aligned}\right\} \tag{2.6}$$

where the asterisk denotes the complex conjugate. Here the matrices T^{mn} and R^{mn} are given by

$$T^{mn} = \begin{pmatrix}\omega^2\sin^2\Phi + f^2\cos^2\Phi & (\omega^2-f^2)\sin\Phi\cos\Phi + i\omega f & -\omega\sin\Phi - if\cos\Phi\\ (\omega^2-f^2)\sin\Phi\cos\Phi - i\omega f & \omega^2\cos^2\Phi + f\sin^2\Phi & -\omega\cos\Phi + if\sin\Phi\\ -\omega\sin\Phi + if\cos\Phi & -\omega\cos\Phi - if\sin\Phi & 1\end{pmatrix} \tag{2.7}$$

and

$$R^{mn} = \varphi_m(k,\omega,z)\,\varphi_n(k,\omega,z'). \tag{2.8}$$

Note that (2.6) is based on the random-phase assumption, i.e.,

$$<\tilde{\zeta}(\boldsymbol{k},\omega)\,\tilde{\zeta}(\boldsymbol{k}',\omega')> = 0 \quad \text{if} \quad \boldsymbol{k}+\boldsymbol{k}' \neq 0 \quad \text{or} \quad \omega+\omega' \neq 0.$$

Changing to a continuous representation, we write:

$$<\tilde{\zeta}(\boldsymbol{k},\omega)\,\tilde{\zeta}^*(\boldsymbol{k},\omega)> \doteq E(\boldsymbol{k},\omega)\,d\boldsymbol{k}\,d\omega. \tag{2.9}$$

The relationship of the spectrum, $E(\boldsymbol{k},\omega)$, to the energy density of the internal-wave field will be pointed out later; see (2.26). The cross-spectral matrix, $A^{mn}(\boldsymbol{r},z,z',\omega)$, which is the Fourier transform of H^{mn} with respect to time, is then given by

$$A^{mn}(\boldsymbol{r},z,z',\omega) = \int E(\boldsymbol{k},\omega)\,T^{mn}\,R^{mn}\,e^{-i\boldsymbol{kr}}\,d\boldsymbol{k}. \tag{2.10}$$

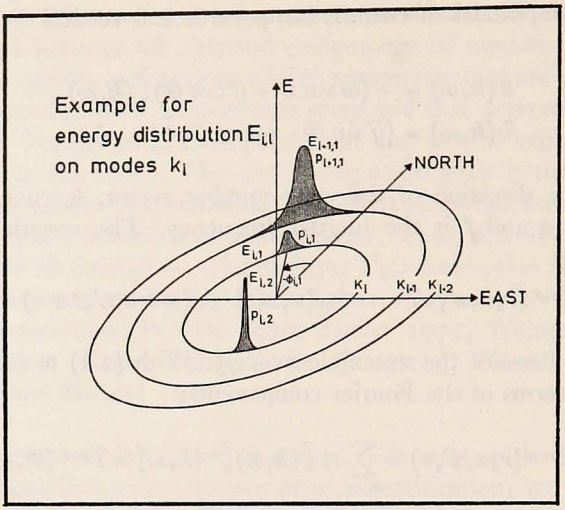

Figure 1.

The eigenfunction concept implies an energy distribution, which is concentrated on circles in the wave-number plane with radius $k_j(\omega), (j = 0, 1, 2, \ldots)$. We assume that the main contribution is due to only a few modes:

$$E(\boldsymbol{k}) = \sum_{j=0}^{N} \frac{E_j}{k_j} S_j(\Phi)\, \delta(k - k_j). \tag{2.11}$$

$S_j(\Phi)$ is the directional distribution on the $_j$th circle and is normalized by

$$\int_0^{2\pi} S_j(\Phi)\, d\Phi = 1. \tag{2.12}$$

Hence,

$$\int E(\boldsymbol{k})\, d\boldsymbol{k} = \sum_{j=0}^{N} E_j. \tag{2.13}$$

From now on, the dependence of all quantities on ω is no longer indicated.

In Fig. 1, a possible energy distribution is sketched. From (2.10) and (2.11), we obtain

$$A^{mn}(\boldsymbol{r}, z, z') = \sum_{j=0}^{N} E_j R_j^{mn} \int_0^{2\pi} S_j(\Phi)\, T^{mn}(\Phi)\, e^{-ik_j r \cos(\Phi - \alpha)}\, d\Phi, \tag{2.14}$$

where

$$R_j^{mn} = R^{mn}(k = k_j), \quad \boldsymbol{r} = (r, \alpha).$$

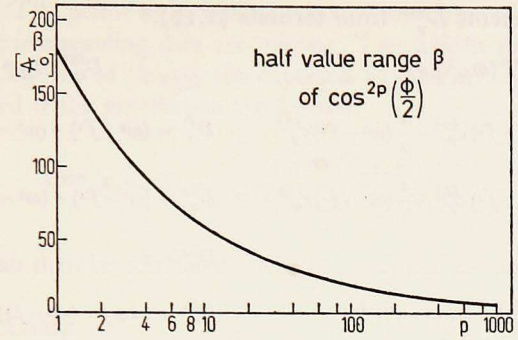

Figure 2.

We now approximate the directional distribution, $S_j(\Phi)$, by a two-parameter function. A convenient choice that permits the analytical evaluation of the integral in (2.14) is

$$S_j(\Phi) = \sigma_j \cos^{2p_j}\left(\frac{\Phi - \Phi_j}{2}\right). \tag{2.15}$$

Here Φ_j stands for the mean propagational direction and p_j is related to the beam width, β_j, by $\cos^{2p_j}\beta_j/4 = 1/2$ (see Fig. 2); σ_j is determined by (2.12). Isotropic energy distribution is represented by $p_j \to 0$, a discrete plane wave by $p_j \to \infty$. A similar function has been used by Barnett (1969) for surface-wave directional spectra.

Furthermore, the case of a more complicated energy distribution may be approximated by using a sum of beams of the type (2.15), with different energies and different mean propagational directions:

$$S_j(\Phi) = \frac{1}{E_j}\sum_{l=1}^{N_j} E_{jl}\,\sigma_{jl}\cos^{2p_{jl}}\left(\frac{\Phi - \Phi_{jl}}{2}\right). \tag{2.16}$$

It seems that the actual energy distribution in the sea may be fairly well described by either (2.15) or (2.16). For simplicity of notation, in the following considerations we use (2.15) instead of the more general (2.16).

The integral in (2.14),

$$I_j^{mn} = \int_0^{2\pi} S_j(\Phi)\,T^{mn}(\Phi)\,e^{-ik_j r\cos(\Phi-\alpha)}\,d\Phi, \tag{2.17}$$

with $S_j(\Phi)$ from (2.15), can be evaluated in terms of Bessel functions:

$$I_j^{mn}(r,\alpha,\Phi_j,p_j) = \frac{1}{2}\left[D_0^{mn}(\Phi_j,p_j)\cdot\mathcal{J}_0(k_j r) + 2\sum_{\nu=1}^{\infty} D_\nu^{mn}(\Phi_j,p_j,\alpha)\,i^\nu\mathcal{J}_\nu(k_j r)\right]. \tag{2.18}$$

Table I. Coefficients D_ν^{mn} from formula (2.18).*

$D_\nu^{mn}(\Phi_j, p_j, \alpha)$	$D_0^{mn}(\Phi_j, p_j)$
$D_\nu^{11} = \frac{1}{2}(\omega^2+f^2)c_\nu^{(0)} - \frac{1}{2}(\omega^2-f^2)c_\nu^{(2)}$	$D_0^{11} = (\omega^2+f^2) - (\omega^2-f^2)\gamma_2 \cos 2\Phi_j$
$D_\nu^{22} = \frac{1}{2}(\omega^2+f^2)c_\nu^{(0)} + \frac{1}{2}(\omega^2-f^2)c_\nu^{(2)}$	$D_0^{22} = (\omega^2+f^2) + (\omega^2-f^2)\gamma_2 \cos 2\Phi_j$
$D_\nu^{33} = c_\nu^{(0)}$	$D_0^{33} = 2$
$D_\nu^{12} = i\omega f c_\nu^{(0)} + \frac{1}{2}(\omega^2-f^2)s_\nu^{(2)}$	$D_0^{12} = 2i\omega f + (\omega^2-f^2)\gamma_2 \sin 2\Phi_j$
$D_\nu^{13} = -\omega s_\nu^{(1)} - if c_\nu^{(1)}$	$D_0^{13} = 2\gamma_1(-\omega \sin\Phi_j - if\cos\Phi_j)$
$D_\nu^{23} = -\omega c_\nu^{(1)} + if s_\nu^{(1)}$	$D_0^{23} = 2\gamma_1(-\omega\cos\Phi_j + if\sin\Phi_j)$

$$D_\nu^{mn} = D_\nu^{nm*}$$

$$\gamma_0 = 1, \gamma_{\nu+1} = \gamma_\nu \frac{p_j - \nu}{p_j + \nu + 1}$$

$$\begin{Bmatrix} s_\nu^{(r)} \\ c_\nu^{(r)} \end{Bmatrix} = \gamma_{\nu+r} \begin{matrix} \sin \\ \cos \end{matrix} (r\Phi_j - \nu[\alpha - \Phi_j - \pi]) + \gamma_{\nu-r} \begin{matrix} \sin \\ \cos \end{matrix} (r\Phi_j + \nu[\alpha - \Phi_j - \pi])$$

* The values for $\nu = 0$ are given explicitly, since only these coefficients are used in some special cases, e.g., formulas (2.22)–(2.24).

The coefficients D_ν^{mn} are listed in Table I. The splitting up of (2.14) into the real part and imaginary part leads to the co-spectrum, C^{mn}, and the quadrature-spectrum, Q^{mn}:

$$A^{mn} = C^{mn} - iQ^{mn} = \sum_{j=0}^{N} E_j R_j^{mn}(z, z') I_j^{mn}(r, \alpha, \Phi_j, p_j). \qquad (2.19)$$

The parameters E_j, Φ_j, p_j can now be determined by fitting (2.19) to the observed co-spectra C_{obs}^{mn} and the quadrature-spectra Q_{obs}^{mn}. Suppose that the cross spectra from a number of M moored instruments are available for the analysis; i.e., the maximum possible number of cross spectra is $S = 9 \cdot M(M+1)/2$.

For a least-squares fit, it is necessary that

$$F(E_0 \ldots E_N, \Phi_0 \ldots \Phi_N, p_0 \ldots p_N) = \sum_{s=1}^{S}{}' \lambda_s \Big\{ \Big[C_{\text{obs}}^{m_s n_s}(r_s, \alpha_s, z_s, z_s') - \\ - C^{m_s n_s}(\ldots) \Big]^2 + \Big[Q_{\text{obs}}^{m_s n_s}(\ldots) - Q^{m_s n_s}(\ldots) \Big]^2 \Big\} \qquad (2.20)$$

be a minimum. The prime at $\sum$ indicates that some terms of the sum may be omitted if the corresponding data are missing. The weight factors, λ_s, will be discussed later. By use of (2.19), the expected field of the squared coherence can be calculated if the parameters are known:

$$K^{mn}(\boldsymbol{r},z,z') = \frac{|A^{mn}(\boldsymbol{r},z,z')|^2}{A^{mm}(o,z,z)\,A^{nn}(o,z',z')}. \tag{2.21}$$

These values can then be compared with the measured coherence field, K^{mn}_{obs}.

Two Special Cases

(i) Current Data from a Single Mooring. Frequently, records are obtained from single stations equipped with several current meters at different depths. For this case ($r = 0$), (2.19) reduces to

$$A^{mn}(o,z,z') = \frac{1}{2}\sum_{j=0}^{N} E_j R_j^{mn}(z,z')\,D_o^{mn}(\Phi_j,p_j). \tag{2.22}$$

With (2.22), the energies, E_j, and the beam-width parameters, p_j, can be determined; the propagational directions, Φ_j, in this case, only result with a 180° ambiguity, as is seen from the D_o^{mn} for $m = 1,2$ in Table I. This ambiguity can be resolved if the vertical displacement has been measured at least at one depth. However, from the D_o^{mn} it can be seen that the determination of propagational directions based on current measurements with only vertical separations will be almost impossible for near-inertial frequencies because of the factor (ω^2-f^2) with all the Φ_j terms. (This will become obvious in one of our examples discussed later). In case one mode contains all of the energy, it follows from (2.21) and (2.22) that the vertical coherence is $K^{mn}(o,z,z') \equiv 1$.

(ii) Horizontal Cross Spectra. We first consider the case of temperature (i.e., elevation) cross spectra. If we assume for a moment a discrete directional energy distribution of each mode, then (2.19) reads:

$$A^{33}(r,\alpha) = \sum_{j=0}^{N} E_j e^{-ik_j r\cos(\Phi_j-\alpha)}. \tag{2.23}$$

This form has been used by one of us in fitting horizontal temperature cross spectra from the North Sea (referred to below) with a single-plane wave. Another interesting relationship holds for the horizontal cross spectra of the individual current components if isotropic energy distribution is assumed:

$$A^{11}_{22}(r,\alpha) = \sum_{j=0}^{N} E_j\left\{\mathcal{J}_0(k_j r) \mp \frac{\omega^2-f^2}{\omega^2+f^2}\cos 2\alpha\,\mathcal{J}_2(k_j r)\right\}\cdot\frac{1}{2}(\omega^2+f^2). \tag{2.24}$$

This special case is the same as that in Garrett and Munk's model except that they do not consider the modal structure. They neglect the second term of (2.24), which seems justified only if the sensor separation is sufficiently small or if near-inertial frequencies are treated.

KINETIC AND POTENTIAL ENERGY. From the parameters determined by the cross-spectral fit, the energy profile and the r.m.s. amplitudes can be calculated. The average total energy per volume in the internal-wave field at depth z is

$$U(z) = \frac{1}{2}\bar{\varrho}(z)<u^2+v^2+w^2+N^2\zeta^2> \tag{2.25}$$

With (2.1), (2.4), and (2.9), the spectral-energy density is given by

$$U(\boldsymbol{k},\omega,z) = \frac{1}{2}\bar{\varrho}(z)E(\boldsymbol{k},\omega)\left[\frac{\omega^2+f^2}{k^2}\left(\frac{d\psi}{dz}\right)^2+(\omega^2+N^2)\psi^2\right]. \tag{2.26}$$

The energy per frequency interval results with the use of (2.11):

$$U(\omega,z) = \frac{1}{2}\bar{\varrho}(z)\sum_{j=0}^{N} E_j\left[\frac{\omega^2+f^2}{k_j^2}\left(\frac{d\psi_j}{dz}\right)^2+(\omega^2+N^2)\psi_j^2\right], \tag{2.27}$$

where $\psi_j \equiv \psi(k_j,\omega,z)$. The first part of this sum, which corresponds to the horizontal kinetic energy, can readily be compared with measured profiles. If the eigenfunctions are normalized according to

$$\int_0^H \bar{\varrho}(z)\left(\frac{d\psi_j}{dz}\right)^2 dz = k_j^2 \tag{2.28}$$

(with H water depth), the contribution of a mode to the horizontal kinetic energy of the water column is directly proportional to E_j.

The mean-square values of the current components and the vertical elevation are given by

$$\left.\begin{aligned}\left\{\begin{matrix}<u^2>\\<v^2>\end{matrix}\right\} &= \sum_{j=0}^{N}\frac{E_j}{k_j^2}\left(\frac{d\psi_j}{dz}\right)^2\left[(\omega^2+f^2)\mp(\omega^2-f^2)\cdot\right.\\ &\qquad\left.\cdot\frac{p_j(p_j-1)}{(p_j+1)(p_j+2)}\cos 2\Phi_j\right]\cdot\Delta\omega,\\ <\zeta^2> &= \sum_{j=0}^{N} 2E_j\psi_j^2\Delta\omega,\end{aligned}\right\} \tag{2.29}$$

with $\Delta\omega$ being the frequency increment. From (2.29) it is seen that $<u^2> = <v^2>$ in the isotropic case ($p_j = 0$); for $p_j \leq 1$, this relationship also holds fairly well.

Weight Factors. For the application of the cross-spectral fit, weight factors had to be introduced in (2.20) for two different reasons: First, not all of the elements of the cross-spectral matrix have the same dimension, since the time series on which the cross spectra are based may consist of velocities and lengths. Second, observed cross spectra of equal dimension may differ considerably in magnitude. In the first case, the difficulty may be resolved by rescaling the vertical elevation, ζ, to obtain a quantity that has the dimension of a velocity and the order of magnitude of the horizontal current. This scaling factor, for example, might be chosen as $\omega\{(\bar{N}^2-\omega^2)/(\omega^2-f^2)\}^{1/2}$, where $\bar{N}$ is an average value of the Brunt-Väisälä frequency.

Another possibility is the normalization by the corresponding autospectra, i.e.,

$$\lambda_s = [C_{\text{obs}}^{m_s m_s}(o, z_s, z_s) \cdot C_{\text{obs}}^{n_s n_s}(o, z_s', z_s')]^{-1}. \tag{2.30}$$

This type of scaling makes all terms of the sum (2.20) dimensionless and of the same order of magnitude. Hence, it is prevented that the approximation fits well to only a few large cross spectra and rather badly to a great number of smaller ones. Therefore, scaling with (2.30) seems reasonable, and we use this procedure in our application to ocean measurements.

Consideration of Errors. Having determined the minimum of (2.20), we are left with a minimum value $F_{\min}$, which usually is not zero; in a sense its value may be regarded as a measure of the quality of the approximation. The ratio of $F_{\min}$ to the (weighted) sum of the squared observed cross spectra, F_o, may provide some idea of the extent to which the data are explained by the model. The deviation from zero minimum may be due to different sources of error, which we now briefly discuss.

Fixed Phases. The different modes may have fixed phase relationships. This may happen near bottom slopes where barotropic wave energy is transformed into baroclinic modes (Rattray et al. 1969). Also, the phases obviously will tend to become more and more fixed if the length of the record is shortened. Application of (2.20) to synthetic data made up of a few modes with fixed phases has revealed that at least the propagational directions were found almost correctly whereas the fitted energies turned out to be rather bad. Therefore, to get reasonable results from the cross-spectral fit, the random-phase condition must not be too heavily violated.

Nonstationarity. To fulfil our stationarity assumption, it may be necessary sometimes to cut longer records into pieces, otherwise propagation characteristics of different processes might get mixed up. The length of a piece has to be a compromise between this requirement and the random-phase condition.

Nonlinearity. Nonlinear interactions transfer energy among different components of the internal-wave field. This means that the energy will remain

on circles in the wave-number plane according to (2.11) while the parameters E_j, Φ_j, p_j may change with time and may thus add to the nonstationary character of the energy spectrum.

NONHOMOGENEITY. This may be due to the topography or to the horizontal distribution of the generating forces. In this case, horizontal separations of the sensors have to be kept sufficiently small with the accompanying disadvantages concerning the spectral resolution.

TURBULENCE. The turbulence spectra may be expected to be rather smooth in the wave-number plane and would therefore add a sort of white noise to the internal-wave field data. The turbulence contribution can be treated together with other unsystematic errors.

DOPPLER EFFECT. The influence of a mean current will result in a deformation of the circular-energy distribution in the wave-number plane. This will be disregarded here.

ALIASING. For the conventional spectral estimators, aliasing plays an important role. Considerable improvement has been achieved by use of the high-resolution method of Capon (1969). In our cross-spectral fit, aliasing corresponds to secondary minima. To be sure that the true minimum is found, the minimum-seeking procedure has to be repeated several times, starting from different initial values of the parameters. From our experience with the cross-spectral fit, secondary minima seem not to be a severe problem. This is partly due to the assumed modal structure of the internal-wave field and partly to the great number of cross spectra available by the combination of all three components of motion, i.e., the great number of degrees of freedom.

In order to quantify error bars of our determined parameters, E_j, Φ_j, p_j, we assume now that the errors in the measurements are largely nonsystematic. The sum (2.20) may be rewritten as

$$F(\mu_1 \cdots \mu_{3(N+1)}) = \sum_{s=1}^{2S}{}' \lambda_s [\chi_s^{\text{obs}} - \chi_s(\mu_1 \cdots \mu_{3(N+1)})]^2, \qquad (2.31)$$

with $\mu_1 \cdots \mu_{3(N+1)}$ being the $^3(N+1)$ parameters (E_j, Φ_j, p_j), $j = 0 \ldots N$ and with $\chi_s^{\text{obs}}, \chi_s$ denoting the observed and theoretical co-spectra $C^{m_s n_s}(r_s, \alpha_s, z_s, z_s')$ for $1 \le s \le S$ and the corresponding quadrature-spectra $Q^{m_s n_s}(\ldots)$ for $S+1 \le s \le 2S$, respectively. In order to apply the standard error calculation of linear least-squares approximation, (2.31) is expanded in the vicinity of the minimum:

$$F = \sum_{s=1}^{2S}{}' \lambda_s \left[\chi_s^{\text{obs}} - \chi_s(\bar{\mu}_1 \cdots \bar{\mu}_{3(N+1)}) - \sum_{l=1}^{3(N+1)} \frac{\partial \chi_s}{\partial \mu_l} (\mu_l - \bar{\mu}_l) \right]^2. \qquad (2.32)$$

Defining the matrix

$$a_{il} = \sum_{s=1}^{2S}{}' \lambda_s \frac{\partial \chi_s}{\partial \mu_i} \frac{\partial \chi_s}{\partial \mu_l}, \quad i, l = 1 \ldots 3(N+1),$$

the r.m.s. deviations $\Delta\mu_s$ are given by

$$\Delta\mu_l = \left[(a)_{ll}^{-1} \frac{F_{\min}}{L} \right]^{1/2}, \tag{2.33}$$

where L is the number of degrees of freedom (Zurmühl 1965). This number is equal to the number of observed co-spectra and quadrature-spectra minus the number of fitting parameters.

If the distribution of the observed cross spectra were known to be Gaussian, the minimum values, $\bar{\mu}_l$, would be t-distributed, with L degrees of freedom; and, from (2.33), confidence limits for the parameters could be calculated. Generally, the observed cross spectra cannot be expected to have a normal distribution. However, if the number of degrees of freedom is sufficiently large, say, 100, the $\bar{\mu}_l$ will approach a normal distribution for *any* distribution of the data.

Typically, the number of degrees of freedom will be this order of magnitude. As an example, assume that the cross spectra from five current meters (60 co-spectra and 40 quadrature-spectra) are used. With a three-mode fit with three fitting parameters each, the number of degrees of freedom is 91.

3. *Application to Internal Tides.* (i) Current and temperature Data from an Array in the North Sea. In the northwestern North Sea, about 100 n.m. off the eastern English Coast (Fig. 3a), currents and temperature fluctuations were recorded for 13 days in September 1968 at four moorings (Fig. 3b). The water depth was 82 m. The density profile was almost two-layered, with a sharp thermocline centered at a depth of about 32 m (Fig. 3c). These data have been discussed elsewhere (Schott 1971a). They should provide a good means of checking our cross-spectral fit, since the tidal parameters may be deduced from different sets of independent cross spectra from different instruments. We use the horizontal cross spectra of the temperature fluctuations at the four stations; separately we use the cross spectra of the currents measured at the central mooring (the best-equipped mooring) and another nearby mooring.

Horizontal Cross Spectra of Temperature Fluctuations. A major difficulty in using the temperature spectra is the sharpness of the thermocline. In the ideal case of a completely two-layered medium, harmonic thermocline waves would be recorded by near-thermocline sensors as rectangular pulses. In our case, where there is a small transition zone between the two layers,

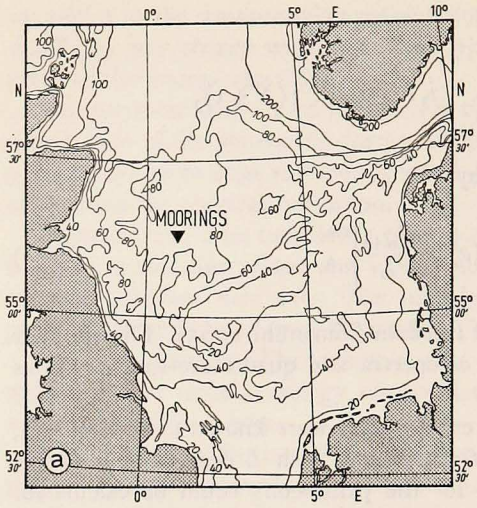

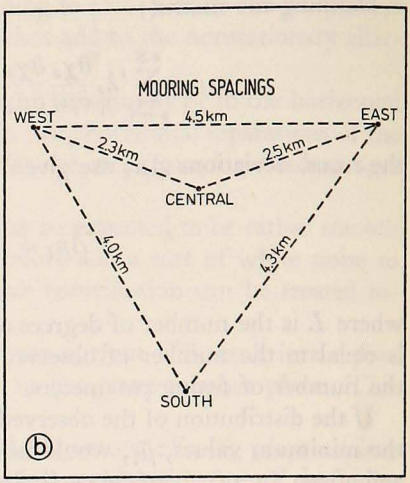

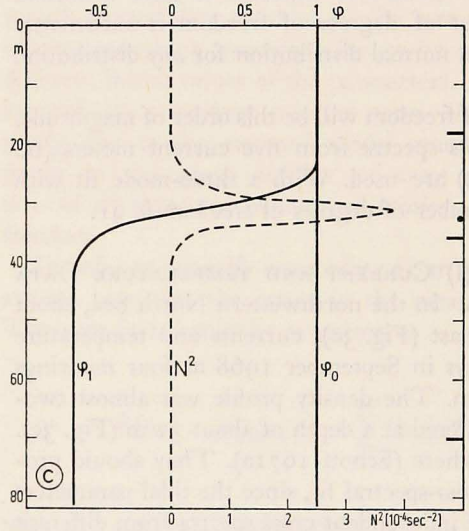

Figure 3. (a) Location of the mooring array in the northwestern North Sea.
(b) Distances between moorings.
(c) Profiles of N^2 (dashed line) and the current eigenfunctions, φ_0 and φ_1 (solid lines). Instrument depths for currents (—) and temperatures (·) are marked on the right ordinate.

the sensors within the thermocline may get, during part of the wave periods, into the homogeneous upper or lower layer; this then results in a cut-off of high amplitudes. Also, this effect will be quite different for sensors that have only a few decimeters of vertical separation. For such a density profile, only

Table II. Fitting parameters (modal energy, E_i, propagation direction, Φ_i) and beam width, β_i), mean-square horizontal currents, and vertical elevations of two modes calculated from the North Sea records.

Fitting parameters	Current ellipse major axis (cm/sec)	Current ellipse minor axis (cm/sec)	Vertical elevation
Barotropic mode			
$k_0 = 6.10^{-3}\text{km}^{-1}$			
$E_0 = 4.09 \pm 0.24$			31 cm
$\Phi_0 = 214° \pm 2°$	12.2	1.7	(surface)
$\beta_0 < 5°$	(contra solem)		
First baroclinic mode			
$k_1 = 0.18\ \text{km}^{-1}$	upper layer:		
$E_1 = 0.45 \pm 0.15$	3.1	2.7	133 cm
$\Phi^{**} = 222° \pm 80°$	lower layer:		(thermocline)
$\beta^{**} = 180° \pm 180°$	1.7	1.5	
$\Phi^{*} = 3° \pm 15°$			

* From temperature cross spectra. ** Uncertain; see text.

the barotropic mode and the first baroclinic mode of tidal waves are important. The above-mentioned difficulties prevent an accurate determination of the energies of both modes from temperature fluctuations, but nevertheless, the propagation direction of the first mode should be almost correct. In fact, our two-mode model gave a northward propagating first mode ($\Phi_1 = 3°$) according to Schott's (1971a) single plane-wave approximation. Introduction of an additional second mode revealed that it was unimportant.

Current Cross Spectra. The current records from four current meters have been used for the fit: three were on the central mooring at depths of 18.5 m, 36.0 m, and 70.0 m and one was on the eastern mooring, 2.5 km away, at a depth of 18.3 m. This provides us with 40 cross-spectra pairs.

An essential relationship for the current cross-spectral fit is (2.4), which means that the main axes of the current ellipse of the modes must have the ratio f/ω. However, the barotropic tide in the North Sea is not such a free wave. Its actual ellipse can be determined by regarding this ratio as a new parameter whose value is to be found in the cross-spectral fit.

The fitting parameters of the barotropic mode and the first baroclinic mode —i.e., the relative energies, E_j, the mean propagational directions, Φ_j, and the beam widths, β_j—are presented in Table II. The barotropic parameters result with remarkably small errors; the axis ratio and the orientation of the major axis are in agreement with the numerical calculations of Hansen (1952) for the M_2 tide in the North Sea. The determination of the baroclinic propagational direction and beam width from these current data must be uncertain

Table III. Squared coherence for sensor pairs and current components, u,v, from North Sea stations East (E) and Central (C). Left-hand columns: data coherence. Right-hand columns: model coherence.

	Current components							
	u–u		u–v		v–u		v–v	
Sensor pairs	Data	Model	Data	Model	Data	Model	Data	Model
E 18.5–E 18.5...	–	–	0.69	0.61	0.69	0.61	–	–
–C 18.3...	1.00	0.98	0.66	0.63	0.76	0.59	0.94	0.99
–C 36.0...	0.60	0.50	0.79	0.77	0.85	0.86	0.77	0.71
–C 70.0...	0.64	0.50	0.84	0.77	0.85	0.86	0.78	0.71
C 18.3–C 18.3...	–	–	0.73	0.61	0.73	0.61	–	–
–C 36.0...	0.61	0.49	0.72	0.78	0.86	0.85	0.76	0.71
–C 70.0...	0.64	0.49	0.77	0.78	0.86	0.85	0.77	0.71
C 36.0–C 36.0...	–	–	0.85	0.83	0.85	0.83	–	–
–C 70.0...	0.89	1.00	0.84	0.83	0.88	0.83	0.97	1.00
C 70.0–C 70.0...	–	–	0.87	0.83	0.87	0.83	–	–

because of the following effects. On the one hand, the axis ratio of the free wave is $f/\omega = 0.87$, which means that the current ellipse does not differ much from a circle. As mentioned in § 2, the theoretical current cross spectra for the vertical separation (at station Central) are then rather insensitive to these two parameters. On the other hand, there is only one small horizontal separation (between Central and East) that provides phase information; and the baroclinic energy is only about one tenth of the barotropic energy. Therefore, the Φ_1 value, determined from the horizontal temperature cross spectra, can be regarded as the more reliable and is inserted in Table II. The ratio $F_{\min}/F_0$ of the fit was 10%.

The possibility of combining temperature and current data, which would allow the determination of unambiguous propagational directions from the Central mooring alone, was investigated but could not be used because of the above-mentioned cut-off effects in the temperature records. A comparison of the observed and model coherences for the four current meters is presented in Table III. The interesting feature is that the coherence across the thermocline is reduced considerably although the first-mode energy is so small compared with the barotropic one.

(ii) Current Cross Spectra from a Single Mooring. This mooring was near the Great Meteor Seamount in the North Atlantic (Figs. 4a, 4b), at a water depth of 4650 m, and was equipped with four current meters at depths of 142 m, 1202 m, 2052 m, and 3002 m. The results of the cross-spectral fit with three modes for all auto spectra and cross spectra of the four instruments (i.e., more than 50 degrees of freedom), using the eigenfunctions in Fig. 4c, are presented in Table IV. The E_j are the relative energies of the modes, with the first baroclinic mode dominant. (The eigenfunctions are nor-

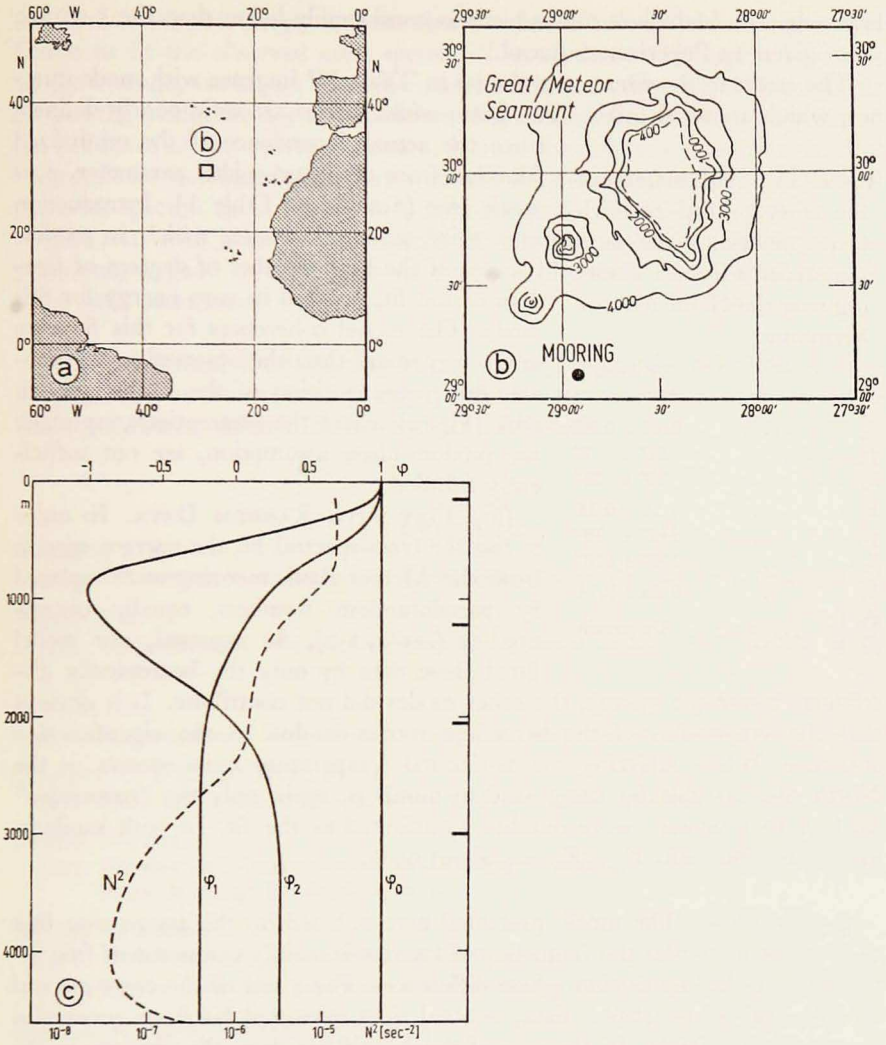

Figure 4. (a) Location of the Great Meteor Seamount in the Atlantic.
(b) Topography of the Seamount and the location of the mooring.
(c) Profiles of N^2 (dashed line) and the current eigenfunctions, φ_0, φ_1, φ_2 (solid line). Current-meter depths are marked on the right ordinate.

malized according to $\psi_j'(0) = k_j$.) For the barotropic mode, the orientation of the current ellipse coincides with the results of Meincke (1971), who fitted the barotropic and the first two baroclinic tidal modes to the individual current Fourier components, and is in fair agreement with the numerical computation by Pekeris and Accad (1969). The current amplitude of 2 cm/sec was a little

lower than in Meincke's results but was considerably lower than the 5 cm/sec value given by Pekeris and Accad.

The errors in the parameters shown in Table IV increase with mode number, which seems plausible. The beam-width values are only poorly defined, since the actual dependence of the minimized function from the beam-width parameter, p, is weak [see (2.22) and Table I]. Introduction of a third baroclinic mode, which is possible because of the high number of degrees of freedom of the fit, resulted in zero energy for this mode. The model coherences for this fit were lower in general than the observed ones, probably due to the position of the mooring in an area (Fig. 4) where the assumptions, especially the random-phase assumption, are not sufficiently fulfilled.

Table IV. Parameters of the cross-spectral fit with three modes to the current records from a mooring near the Great Meteor Seamount.

	Fitting parameters
E_0	0.36 ± 0.07
Φ_0	$61° \pm 7°$
β_0	$30° \pm 25°$
E_1	1.54 ± 0.41
Φ_1	$242° \pm 78°$
β_1	$130° \pm 110°$
E_2	0.26 ± 0.11
Φ_2, β_2	Uncertain

(iii) Test with Random Data. In order to test the cross-spectral fit, the current spectra from the Meteor Bank mooring were replaced by pseudorandom numbers, equally distributed in $(-1/2, 1/2)$. As expected, our model fitted these data by only the isotropically distributed barotropic energy, the other modes did not contribute. It is obvious that the suppression of the baroclinic modes is due to the eigenfunction structure. When replacing the horizontal temperature cross spectra in the North Sea example by using random numbers, again only the "barotropic" mode with near-zero wave number contributed to the fit. In both random-data tests, the ratio $F_{\min}/F_0$ was about 90%.

4. *Conclusions.* The model presented here is based on the assumption that the field of motion at the frequency of interest is mainly composed of free internal waves having random-phase differences. For a test of the cross-spectral fit with real oceanographic data, internal tides measured far from generation areas seemed suitable. In the case of the North Sea data, the distance to the probable generation area (the slopes in the southern North Sea) of the northward propagating baroclinic mode is of the order of several first-mode wavelengths. A continuous phase change between the barotropic and baroclinic tidal waves has been found by piecewise Fourier analysis, i.e., the requirement of random-phase differences can be assumed to be met. The observed vertical and horizontal coherences are well explained with the two-mode model. The remarkable fact is that the presence of the baroclinic mode, though only one tenth of the barotropic energy, results in a decrease of the squared vertical coherence across the thermocline down to 0.50. In the deep-sea example, a

few modes—the barotropic and the first two baroclinic modes—are again sufficient to fit the observed cross spectra. The observed coherences, however, on the average, are higher than the model coherences. One explanation might be that the modes are not to a sufficient degree statistically independent due to the influence of the nearby seamount. Hence, these deep-sea data are no ideal "test set" for our model, but they were the only ones at hand. Application of the cross-spectral fit to Site-D data is in progress.

The tests with random data support the conclusion that, at least in our applications, a good cross-spectral fit provides physically meaningful internal wave-field parameters.

Acknowledgment. During a stay by one of us (F.S.) at the GFD Seminar in Woods Hole in the summer of 1972, helpful comments were contributed by Willem Malkus, Melvin Stern, and Carl Wunsch.

REFERENCES

Barnett, T. P.
1969. Wind waves in shallow water. Westinghouse Ocean Res. Lab., San Diego. 56 pp.

Capon, J. R.
1969. High-resolution frequency-wavenumber spectrum analysis. Proc. IEEE, 57(8): 1408–1418.

Eckart, Carl
1960. Hydrodynamics of oceans and atmospheres. Pergamon Press, New York. 290 pp.

Garrett, C. J. R., and W. H. Munk
1972. Space-time scales of internal waves. Geophys. fluid Dynam., 2: 225–264.

Hansen, Walter
1952. Gezeiten und Gezeitenströme der halbtägigen Hauptmondtide M_2 in der Nordsee. Dtsch. Hydrogr. Z., Erg.h. 1; 46 pp.

Krauss, Wolfgang
1963. Zum System der internen Seiches der Ostsee. Kiel. Meeresforsch., 19: 119–132.
1969. Typical features of internal wave spectra. Progr. in Oceanogr., 5: 95–101.

Magaard, Lorenz, and William McKee
Semi-diurnal tidal currents at "Site D". Submitted to Deep-sea Res.

Meincke, Jens
1971. Der Einfluss der Grossen Meteorbank auf Schichtung und Zirkulation der ozeanischen Deckschicht. "Meteor" Forsch.-Ergebn. A(9): 67–94.

Munk, W. H., and N. A. Phillips
1968. Coherence and band structure of inertial motion in the sea. R. Geophys., 6: 447–472.

Pekeris, C. L., and Y. P. Accad
1969. Solution of Laplace's equation for the M_2 tide in the world ocean. Phil. Trans. R. Soc., A 265: 413–436.

PERKINS, H. T.
1970. Inertial oscillations in the Mediterranean. Ph. D. Thesis, M.I.T. and W.H.O.I.; 155 pp.

RATTRAY, Jr., MAURICE, J. G. DWORSKI, and P. E. KOVALA
1969. Generation of long internal waves at the continental slope. Deep-sea Res., Suppl. *16*: 179–195.

SCHOTT, FRIEDRICH
1971a. On horizontal coherence and internal wave propagation in the North Sea. Deep-sea Res., *18*: 291–307.

1971b. Spatial structure of inertial period motions in a two-layered sea, based on observations. J. mar. Res., *29*: 85–102.

SIEDLER, GEROLD
1971. Vertical coherence of short-periodic current variations. Deep-sea Res., *18*: 179–191.

In press. Observations of internal wave coherence and fine-structure contamination in the deep ocean.

WEBSTER, FERRIS
1972. Estimate of the coherence of ocean currents over vertical distances. Deep-sea Res., *19*: 35–44.

WUNSCH, C. I., and J. H. DAHLEN
1970. Preliminary results of internal wave measurements in the main thermocline at Bermuda. J. geophys. Res., *75*: 5899–5908.

WUNSCH, C. I., and R. C. HENDRY
1972. Array measurements of the bottom boundary layer and the internal wave field on the continental slope. Geophys. fluid Dyn., *4*: 101–145.

ZALKAN, R. L.
1970. High frequency internal waves in the Pacific Ocean. Deep-sea Res., *17*: 91–108.

ZURMÜHL, RUDOLF
1965. Praktische Mathematik. Springer-Verlag, Berlin. 561 pp.